

# GAN Inversion for Image Editing via Unsupervised Domain Adaptation

Siyu Xing<sup>1,4</sup>, Chen Gong<sup>2</sup>, Hwei Guo<sup>3</sup>, Xiao-yu Zhang<sup>1,4,\*</sup>, Xinwen Hou<sup>3</sup>, Yu Liu<sup>3</sup>

<sup>1</sup>*Institute of Information Engineering, Chinese Academy of Sciences, Beijing, China*

<sup>2</sup>*University of Virginia, Charlottesville, The United States of America*

<sup>3</sup>*Institute of Automation, Chinese Academy of Sciences, Beijing, China*

<sup>4</sup>*School of Cyber Security, University of Chinese Academy of Sciences, Beijing, China*

{xingsiyu, zhangxiaoyu}@iie.ac.cn, chengong@virginia.edu, {guohewei2020, xinwen.hou, yu.liu}@ia.ac.cn

**Abstract**—Existing GAN inversion methods work brilliantly in reconstructing high-quality (HQ) images while struggling with more common low-quality (LQ) inputs in practical application. To address this issue, we propose Unsupervised Domain Adaptation (UDA) in the inversion process, namely UDA-inversion, for effective inversion and editing of both HQ and LQ images. Regarding unpaired HQ images as the source domain and LQ images as the unlabeled target domain, we introduce a theoretical guarantee: loss value in the target domain is upper-bounded by loss in the source domain and a novel discrepancy function measuring the difference between two domains. Following that, we can only minimize this upper bound to obtain accurate latent codes for HQ and LQ images. Thus, constructive representations of HQ images can be spontaneously learned and transformed into LQ images without supervision. UDA-Inversion achieves a better PSNR of 22.14 on FFHQ dataset and performs comparably to supervised methods.

**Index Terms**—GAN (generative adversarial networks), GAN inversion, unsupervised domain adaptation, image editing, StyleGAN

## I. INTRODUCTION

Generative adversarial networks (GANs) have achieved remarkable performance in image generation [1]–[4], which utilize the neural network to synthesize high-quality images in one step. Due to the rich semantics in the latent space of a well-trained GAN (e.g., StyleGAN), controllable image editing can be achieved by altering the latent code of an image generated from GAN [5]–[7]. As presented in Fig. 1 (a), manipulating a latent code  $z_1$  can make a high-quality face image younger or happier. GAN inversion broadens the editing scope from synthesized images to real images. Typically, GAN inversion learns to map a real image back to an inverted code in the latent space of a pre-trained GAN [8]. The inverted code accurately reconstructs the input by the generator and enables the editing of the given image in latent space.

Previous GAN inversion methods focus only on high-quality (HQ) images that are similar to the training set of GANs while ignoring other common images in practice, i.e., low-quality (LQ) images [9]. As depicted in Fig. 1 (a) and (b), employing a low-quality (LQ) image as the input for vanilla GAN inversion [10] often results in a poorly inverted image, in contrast to high-quality (HQ) images. A gap exists between the latent code distributions of HQ and LQ images even in the same latent space. When faced with out of domain images

(usually LQ images), this drawback impedes the progress of GAN inversion in practical applications.

This dilemma motivates GAN community to develop a GAN inversion method for inverting and editing both LQ and HQ images. Previous works [11]–[13] have been proposed to reconstruct LQ input images in a supervised manner, focusing solely on paired HQ-LQ images [11], [12] or degradation information [13], such as the mask that describes the defective region in inpainting task. Images in real-world scenarios are typically affected by various complex and even unknown perturbations, making it difficult for researchers to gather the corresponding paired HQ image in terms of a given LQ image. Thus, inverting LQ images without supervision remains a challenging problem that deserves further exploration.

To address above issues, we propose a novel GAN inversion framework based on Unsupervised Domain Adaptation (UDA), named UDA-inversion. The key insight is to find unbiased latent codes for HQ and LQ images by unsupervised domain adaptation. We regard HQ and LQ images as the source and unlabeled target domains, respectively. Since the semantics in the two domains are quite similar, it is reasonable to use the source distribution to approximate the target distribution. Constructive representation of HQ images in the source domain can be spontaneously learned and transferred to LQ images in the target domain without paired data supervising or degradation information. As illustrated in Fig. 1 (c) and (d), UDA-inversion projects LQ and HQ images to latent space by domain adaptation, after which we can edit images by manipulating latent codes in GAN’s latent space.

In particular, we provide a theoretical guarantee that the reconstruction loss over the target domain is upper-bounded by the loss value in the source domain and the discrepancy between two domain distributions (see Theorem 1). We reformulate the upper bound to calculate this discrepancy simply and efficiently. By minimizing this upper bound, we can obtain the optimal latent code of images from the source and target domains (i.e., HQ and LQ images) and steer the latent code to achieve semantic editing. Experiments on image inversion and editing tasks show that our unsupervised method achieves competitive results on image inversion and editing tasks when compared to supervised methods.

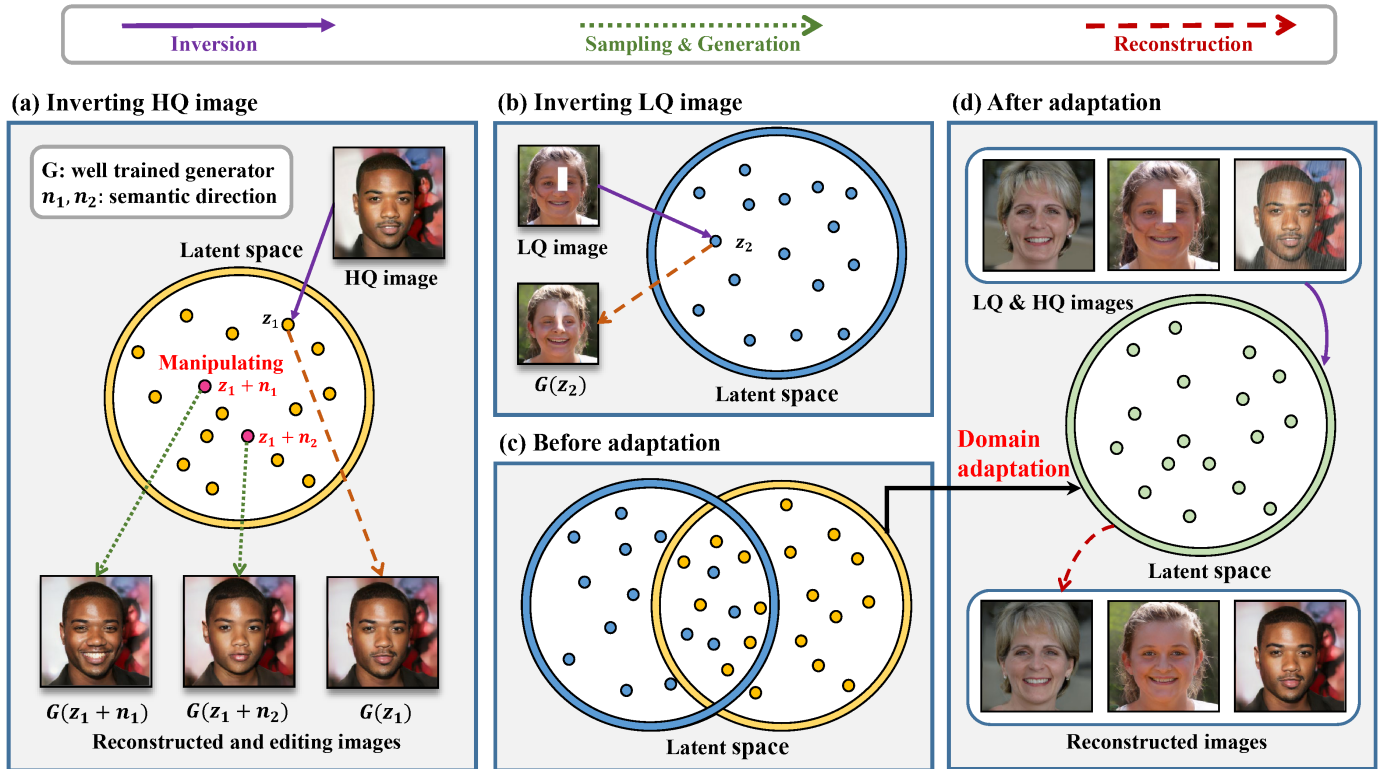


Fig. 1: Overview of existing GAN inversion methods and our UDA-inversion. In subfigure (a), a naive GAN inversion maps HQ image into the latent space of a GAN model and recovers the input with latent code  $z_1$ . Manipulating  $z_1$  in semantic directions can edit the reconstructed image. (b) describes that most classical GAN inversion methods only work on HQ images, and the inverted image is usually inaccurate when inputting LQ image. The image  $G(z_2)$  follows the method presented in [10], a well-established encoder-based method. (c) illustrates that we approximate the LQ images’ latent code distribution by domain adaptation. (d) shows that after adaptation, UDA-inversion obtains photorealistic results given HQ and LQ images.

## II. RELATED WORK

### A. GAN Inversion

GAN inversion methods can be grouped into three categories [8]: optimization-based, encoder-based, and hybrid methods. The optimization-based methods use gradient descent to optimize the latent code for reconstructing the image [14]–[16]. However, the above methods are time-consuming in inference [15] – merely inverting an image requires thousands of iterations. The encoder-based GAN inversion method, which projects images to latent space with an encoder, has presented a better performance in semantic editing [10] and faster inference time. Hybrid methods combine two methods above, using an encoder to provide a better initialization for latent code optimization [10]. Researchers pay attention to promoting the performance of GAN inversion by refining the encoder architecture [11], [12], [17], [18] and focus primarily on HQ images similar to the GAN training dataset, leading to the causes of failure for LQ images. We show that UDA-inversion method obtains the optimal latent codes for both HQ and LQ images through unsupervised domain adaptation.

### B. Image Processing with GAN Inversion

Recent years have witnessed various GAN inversion methods applied in image processing fields, such as image colorization [15], [16] and inpainting [11], [12]. Most methods require training with paired data by LQ images as input and corresponding HQ images as additional supervision [11], [12]. Some optimization-based methods [15], [16] require the advanced known degradation operator so that the reconstructed image after degradation closes to the LQ image. Differently, our method inverts the degraded image to an accurate latent code that can be edited to manipulate the semantics without paired images and advanced known degradation operators.

### C. Manipulating Images in GANs’ Latent Space

Due to the rich semantics in the latent space of StyleGAN [5]–[7], diverse methods are used to manipulate latent codes for specific visual attribute editing without retraining the generator. Shen et al. [6] utilize a pre-trained classifier to identify linear semantic directions in the latent space. Wu et al. [7] discover various channel-wise style parameters from the generator to control different visual attributes. Härkönen et al. [5] utilize typical unsupervised learning strategies to

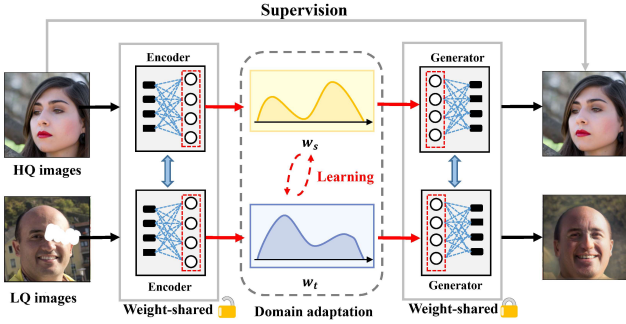


Fig. 2: UDA-inversion consists of a fixed well-trained generator and a trainable encoder, both of which are weight-shared for two domains. Supervision only drives inversion on HQ images. Latent code  $w_t$  of LQ image spontaneously learns and transfers from accurate latent code  $w_s$  of HQ image by unsupervised domain adaptation.

explore underlying semantics in the latent space of pre-trained generators. Overall, editing synthesized images in the latent space of GAN has achieved great success. GAN inversion extends the methods above to real image manipulation. We invert a real image back to a latent code and then directly control the inverted code to obtain desired inversion and editing results.

### III. METHOD

In this section, we first explain problem formulation, after which we construct the total objective of UDA-inversion.

**Problem Formulation.** We assume that  $\mathcal{X}$  is the input data space and  $\mathcal{Y}$  is the label space, e.g.,  $\mathcal{Y}$  is a one-hot vector space for classification. Here,  $\mathcal{Y}$  is an image space for GAN inversion. HQ images in the source domain and LQ images in the target domain are separately drawn from the corresponding distributions  $P_s$  and  $P_t$  over  $\mathcal{X}$ . Since we have access to labeled source samples and unlabeled target samples in unsupervised domain adaptation, and it is impractical to find a HQ image corresponding to the given LQ image, HQ and LQ images are *unpaired* in UDA-inversion training.

We define  $f_s$  and  $f_t: \mathcal{X} \rightarrow \mathcal{Y}$  as the source and target labeling functions, and  $\ell: \mathcal{Y} \times \mathcal{Y} \rightarrow \mathbb{R}^+$  is the loss function that measures the difference between the two labeling functions. Unsupervised domain adaptation intends to find a hypothesis function  $h: \mathcal{X} \rightarrow \mathcal{Y}$  that generalizes to the target domain with error  $R_t^\ell(h) = \mathbb{E}_{\mathbf{x} \sim P_t}[\ell(h(\mathbf{x}), f_t(\mathbf{x}))]$  as small as possible, but we have no knowledge about  $f_t(\cdot)$ .

#### A. UDA-inversion: Unsupervised Domain Adaptation in GAN Inversion

Due to the critical scenarios above, it is impossible to directly minimize error in the target domain. This section presents UDA-inversion to solve this dilemma. Theorem 1 indicates the relationship between two domains, which motivates us to minimize the objective  $R_t^\ell(h)$  via its upper bound.

*Theorem 1 (Generalization Bound [19]):* We suppose  $\ell: \mathcal{Y} \times \mathcal{Y} \rightarrow [0, 1] \subset \text{dom } \phi^*$ . Denote  $\lambda^* := R_s^\ell(h^*) + R_t^\ell(h^*)$ ,

and  $h^*$  be the ideal joint hypothesis function under hypothesis class  $\mathcal{H}$ . Three terms bound the error in the target domain:

$$R_t^\ell(h) \leq R_s^\ell(h) + D_{h, \mathcal{H}}^\phi(P_s \| P_t) + \lambda^*, \quad (1)$$

where  $\phi^*$  denotes the Fenchel conjugate function in terms of a given convex function  $\phi$ . The second term of the right-hand side in (1) is a discrepancy function between two distributions, formulated as:

$$D_{h, \mathcal{H}}^\phi(P_s \| P_t) := \sup_{h' \in \mathcal{H}} | \mathbb{E}_{\mathbf{x} \sim P_s} [\ell(h(\mathbf{x}), h'(\mathbf{x}))] - \mathbb{E}_{\mathbf{x} \sim P_t} [\phi^*(\ell(h(\mathbf{x}), h'(\mathbf{x})))] |. \quad (2)$$

We provide the proof of Theorem 1 and reveal the discrepancy  $D_{h, \mathcal{H}}^\phi(P_s \| P_t)$  serving as a lower bound estimator of the  $f$ -divergence (e.g., KL divergence [1], [20]) in App.A.A -A.B.

The last term of (1) is negligible if the capability of hypothesis space  $\mathcal{H}$  is sufficient, suggesting a convenient way to calculate objectives. It is common in domain adaptation that the ideal joint risk  $\lambda^*$  is small when  $P_s \approx P_t$ , which is also ubiquitous in modern GANs: When latent codes  $w_1$  and  $w_2$  have a negligible difference, the generated images  $G(w_1)$  and  $G(w_2)$  are similar in visual. Thus, the objective in target domain  $R_t^\ell$  can be optimized by simultaneously minimizing the error in the source domain and the discrepancy between two domains in the latent space, which is formulated as:

$$\mathcal{L} = \mathbb{E}_{\mathbf{x} \sim P_s} [\ell(G \circ E(\mathbf{x}), \mathbf{x})] + D_{h, \mathcal{H}}^\phi(P_s^w \| P_t^w), \quad (3)$$

where  $G(\cdot)$  denotes a fixed well-trained generator and  $E(\cdot)$  is an encoder. Two domains' distributions in the latent space are defined as  $P_s^w$  and  $P_t^w$  with densities  $p_s^w$  and  $p_t^w$  respectively, and “ $\circ$ ” indicates the composition operation. As illustrated in Fig. 2, unlike supervised learning [11], [12] with paired images or degradation operator, UDA-inversion can minimize (3) to obtain accurate inversion results for both HQ and LQ images by domain adaptation.

**Loss Functions in Source Domain.** We consider the first item in (3) from the pixel level and other feature levels to achieve reconstruction on the source domain. Specifically, we integrate pixel squared error, LPIPS (Learned Perceptual Image Patch Similarity) [21] and identity features to measure the difference between two images  $\mathbf{x}$  and  $G \circ E(\mathbf{x})$ :

$$\begin{aligned} \mathcal{L}_s &= \mathbb{E}_{\mathbf{x} \sim P_s} [\ell(G \circ E(\mathbf{x}), \mathbf{x})] \\ &= \lambda_1 \mathcal{L}_2 + \lambda_2 \mathcal{L}_{LPIPS} + \lambda_3 \mathcal{L}_{id} \\ &= \mathbb{E}_{\mathbf{x} \sim P_s} [\lambda_1 \ell_2(G \circ E(\mathbf{x}), \mathbf{x}) + \lambda_2 \ell_2(H \circ G \circ E(\mathbf{x}), H(\mathbf{x})) \\ &\quad + \lambda_3 \ell_2(R \circ G \circ E(\mathbf{x}), R(\mathbf{x}))], \end{aligned} \quad (4)$$

where  $\ell_2$  is a squared error.  $H(\cdot)$  is the AlexNet feature extractor in LPIPS, and  $R(\cdot)$  also denotes an identity extractor from a face recognition network [22].

**Discrepancy Between Two Domains.** The next proposition shows how to calculate the intractable discrepancy  $D_{h, \mathcal{H}}^\phi(P_s^w \| P_t^w)$  between two domains in an efficient way.

*Proposition 1:* Let us assume that  $\forall h \in \mathcal{H}, \exists h' \in \mathcal{H}$  s.t.  $\hat{\ell}(h'(\mathbf{w}), h(\mathbf{w})) = \phi'(\frac{p_s^w(\mathbf{w})}{p_t^w(\mathbf{w})})$ , for all latent code  $\mathbf{w} \in \text{supp}(p_t^w(\mathbf{w}))$ . We denotes  $d_{s,t}^w$  as the lower bound of the

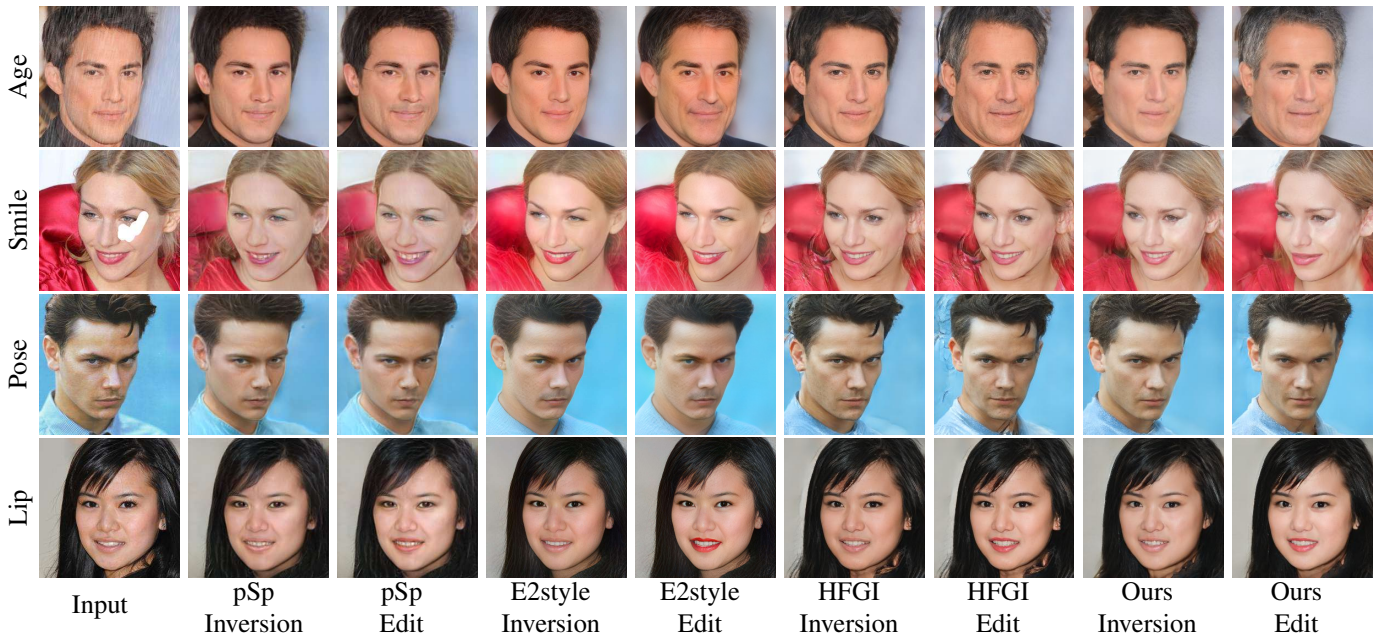


Fig. 3: Qualitative results comparison on image inversion and editing with state-of-the-art GAN inversion methods. From the top to bottom, face images in the first two rows are downgraded by rain layer and random mask. Best viewed zoomed-in.

discrepancy in (5). Maximizing  $d_{s,t}$  can obtain equivalent  $D_{h,\mathcal{H}}^\phi(P_s^w \| P_t^w)$ , i.e.,  $\max_{h' \in \mathcal{H}} d_{s,t} = D_{h,\mathcal{H}}^\phi(P_s^w \| P_t^w)$ .

$$d_{s,t} := \mathbb{E}_{\mathbf{w} \sim P_s^w} \left[ \hat{\ell}(h'(\mathbf{w}), h(\mathbf{w})) \right] - \mathbb{E}_{\mathbf{w} \sim P_t^w} \left[ (\phi^* \circ \hat{\ell})(h'(\mathbf{w}), h(\mathbf{w})) \right]. \quad (5)$$

Here,  $h$  and  $h'$  belong to hypothesis space  $\mathcal{H}$ ,  $\phi^*$  is the Fenchel conjugate function of  $D_{h,\mathcal{H}}^\phi(P_s^w \| P_t^w)$ , and  $\hat{\ell}(h'(\mathbf{w}), h(\mathbf{w})) \rightarrow \text{dom } \phi^*$  indicates the “distance” between two functions. The proof of Proposition 1 is provided in App.A.C. In short, we approximate the intractable discrepancy by solving an optimization problem over  $h'$ :

$$D_{h,\mathcal{H}}^\phi(P_s^w \| P_t^w) = \max_{h' \in \mathcal{H}} \mathbb{E}_{\mathbf{w} \sim P_s^w} \left[ \hat{\ell}(h', h) \right] - \mathbb{E}_{\mathbf{w} \sim P_t^w} \left[ (\phi^* \circ \hat{\ell})(h', h) \right]. \quad (6)$$

To facilitate  $\hat{\ell}$  and  $h$  to measure the similarity between two images, we project inverted images  $G \circ E(\mathbf{x})$  into the representation space of LPIPS [21] to obtain the perceptual similarity between two images. When the generator  $G$  is well-trained and fixed, the discrepancy between two distributions in the latent space is equivalent to the synthesized image space. Thus, according to (6), the discrepancy is reformulated as:

$$\max_{\hat{H}} d_{s,t} = \max_{\hat{H}} \mathbb{E}_{\mathbf{x} \sim P_s} \left[ \hat{\ell}(\hat{H} \circ G \circ E, H \circ G \circ E) \right] - \mathbb{E}_{\mathbf{x} \sim P_t} \left[ (\phi^* \circ \hat{\ell})(\hat{H} \circ G \circ E, H \circ G \circ E) \right], \quad (7)$$

where  $\hat{H}$  indicates a network with the same structure as AlexNet  $H$  in (4) and  $\hat{\ell}$  refers to LPIPS loss, interpreted to

minimize the distance at perceptual feature level. Following proposition 1, we choose the convex function  $\phi$  of Pearson  $\chi^2$  divergence. Detailed discussion is present in App.A.D.

Overall, the objective in (3) is reformulated as:

$$\min_E \max_{\hat{H}} \mathcal{L}_s + \lambda_{uda} d_{s,t}, \quad (8)$$

where  $\lambda_{uda}$  is a hyper-parameter. To optimize the min-max objective in (8), we alternatively update the parameters of  $E$  and  $\hat{H}$  to relieve the unstable gradient burden.

## IV. EXPERIMENTS

### A. Experiment Setting

**Datasets.** We conduct experiments on FFHQ [3] dataset for training and CelebA-HQ [2] test set for evaluation. After assigning the first 50% of images from the training set as data in the source domain (i.e., HQ images), we degrade remaining data as the LQ images in target domain. The degradation operations contain rain layer, random mask, and down-sample, some of which are utilized in existing methods [11], [12]. We use the “RainLayer” feature from the imgaug library [23] with default parameters, perturbing images to a rain effect.

**Implementation Details.** We want to verify that UDA-inversion matches the performance of the state-of-the-art supervised encoder-based GAN inversion methods, i.e., pSp [11], E2style [12], HFGI [18], which are selected as our baselines. To ensure a fair comparison, we retrain these methods with the same source domain as ours and provide additional paired LQ-HQ images from the target domain. We use the pre-trained StyleGAN2 [4] as the generator. We follow existing encoder-based methods [12], [18] with Ranger optimizer [24], [25] during training and set the initial learning rate to 0.0001.

TABLE I: Quantitative comparison of different GAN inversion methods on CelebA-HQ dataset. In the first column, ‘src’ means the evaluation from the source domain, and ‘trg’ means the evaluation from the target domain.  $\uparrow$  means higher is better, and  $\downarrow$  means lower is better.

	PSNR $\uparrow$	SSIM $\uparrow$	FID $\downarrow$	MSE $\downarrow$
HFGI (src)	21.97	<b>0.64</b>	<b>16.97</b>	0.028
HFGI (trg)	21.80	0.63	17.56	0.029
E2style (src)	21.12	0.62	47.90	0.035
E2style (trg)	21.06	0.62	48.34	0.035
pSp (src)	20.37	0.56	46.84	0.040
pSp (trg)	20.32	0.56	46.56	0.040
Ours (src)	<b>22.14</b>	<b>0.64</b>	20.09	<b>0.026</b>
Ours (trg)	20.22	0.62	23.23	0.050

TABLE II: Quantitative comparison of editing results for FID and IDs (Identity similarity). **Bold** indicates the best result. Underline indicates the second-best.

	Methods	Age		Pose		Smile	
		FID $\downarrow$	IDs $\uparrow$	FID $\downarrow$	IDs $\uparrow$	FID $\downarrow$	IDs $\uparrow$
Src	HFGI	<u>57.66</u>	<b>0.45</b>	<u>67.12</u>	<u>0.46</u>	61.64	<u>0.45</u>
	E2style	106.51	0.33	91.84	0.39	84.08	0.37
	pSp	104.61	0.28	70.21	0.25	70.07	0.32
	Ours	<b>57.06</b>	<b>0.45</b>	<b>62.15</b>	<b>0.47</b>	<b>61.19</b>	<b>0.46</b>
Trg	HFGI	<b>59.53</b>	<b>0.41</b>	<u>69.89</u>	<b>0.42</b>	<b>63.40</b>	<b>0.41</b>
	E2style	108.68	0.31	94.42	0.37	85.48	0.36
	pSp	104.53	0.17	70.29	0.24	70.44	0.31
	Ours	<u>60.59</u>	<u>0.40</u>	<b>68.60</b>	<b>0.42</b>	<u>64.82</u>	<b>0.41</b>

The encoder architecture and hyper-parameters are the same as HFGI [18]. Two popular editing methods, GANSpace [5] and InterfaceGAN [6] are selected for semantic editing to manipulate inverted images.

**Evaluation Metrics** We quantitatively evaluate the inversion results from two aspects, i.e., inversion accuracy and image quality [8]. Inversion accuracy is usually measured by PSNR (Peak Signal-to-Noise Ratio), SSIM (Structural Similarity) [26], and MSE (Mean Squared Error). Images generated based on GANs are usually evaluated by FID (Fréchet inception distance) [27] to assess the quality and diversity of image distribution. We introduce IDs (Identity similarity) [28] to evaluate the identity consistency of editing results.

### B. Results and Analysis on Inversion and Editing Tasks

**Qualitative Evaluation.** Figure 3 displays a visualization of the inversion and editing results. The performance of UDA-inversion is comparable to existing supervised methods.

•*Inversion results.* The even columns of Fig. 3 present a qualitative comparison of inverted images. Specifically, pSp [11] and E2style [12] may struggle with reconstructing details, but UDA-inversion can better reconstruct finer details (i.e., 1st, and 3rd rows). Compared to HFGI [18], UDA-inversion better overcomes the artifacts in the background.



Fig. 4: Inversion result of UDA-inversion w/ and w/o  $d_{s,t}$ .

TABLE III: Ablation study of UDA-inversion on target domain, evaluated by PSNR, SSIM, FID, and MSE.

	PSNR $\uparrow$	SSIM $\uparrow$	FID $\downarrow$	MSE $\downarrow$
UDA-inversion	<b>20.22</b>	<b>0.62</b>	<b>23.23</b>	<b>0.05</b>
UDA-inversion w/o $d_{s,t}$	19.01	0.59	31.10	0.06

•*Editing results.* UDA-inversion achieves performance comparable to existing methods. The visual alteration of E2style’s editing varies slightly (e.g., 2nd row), and the background of HFGI editing is distorted (e.g., 2nd row and 3rd row). Our method presents the best visually pleasing editing results among baselines, suggesting that existing supervised methods concentrate on reconstruction, while UDA-inversion generates semantically relevant latent codes through domain adaptation.

**Quantitative Evaluation.** Quantitative results on inversion and editing tasks are presented in TABLE I and TABLE II.

•*Inversion results.* Specifically, UDA-inversion outperforms baselines on PSNR, SSIM, and MSE and achieves comparable results on FID for images in the source domain. The loss function of UDA-inversion on the source domain is similar to baselines, indicating the positive impact of our domain adaptation on source image inversion.

•*Editing results.* We evaluate editing results using FID and IDs (Identity similarity [28]). TABLE II shows a quantitative comparison under the same editing scalar in each attribute. It is noticed that our editing results surpass other baselines in the source domain and achieve competitive results in the target domain, indicating that our method can enhance the ability to understand semantics in GANs’ latent space. Fig. 3 show consistent results with quantitative evaluation.

### C. Additional Analysis

**Ablation Study.** We aim to verify the effectiveness of our major component, i.e.,  $d_{s,t}$  in Eq. (8). As shown in TABLE III and Fig. 4, we examine the corresponding results by comparing two inversion versions: with and without  $d_{s,t}$  (denoted by w/  $d_{s,t}$  and w/o  $d_{s,t}$ , respectively). UDA-inversion alleviates the negative influence of inverted images from LQ images with  $d_{s,t}$ , suggesting that domain adaptation makes the difference between two domains smaller, and our proposed method is more robust to perturbation.

**Additional Experiment.** Table IV reports a qualitative comparison between UDA-inversion and a combination of image reconstruction and GAN inversion, where the former is a blind face restoration method, i.e., DFDNet and GPEN [29], [30]. This comparison highlights the distinction between UDA-

TABLE IV: Qualitative comparison of inversion quality, run time, and model parameters on the CelebA-HQ dataset.

	PSNR $\uparrow$	SSIM $\uparrow$	RunTime(s) $\downarrow$	Param(M) $\downarrow$
DFDNet [29]+HFGI [18]	19.92	0.49	1.05s	395.7
GPEN [30]+HFGI [18]	19.32	0.57	0.54s	288.6
UDA-inversion	<b>20.22</b>	<b>0.62</b>	<b>0.24s</b>	<b>262.4</b>

inversion and a straightforward “A+B” pipeline. By measuring PSNR, SSIM, average run time, and model parameters on the CelebA-HQ test set in TABLE IV, UDA-inversion outperforms this combination in terms of inversion results with faster inference speed and fewer parameters.

## V. CONCLUSIONS

This paper proposes UDA-inversion, a novel encoder-based approach for low-quality GAN inversion without the supervision of paired images or degradation information. We explore how to map HQ and LQ images into the latent space of GAN and derive the underlying knowledge across two distributions by unsupervised domain adaptation. Resolving this problem from domain adaptation, we first regard HQ and LQ images as the source and target domains. Then, we optimize the encoder from the generalization bound of domain adaptation by minimizing the source error and the discrepancy between two distributions in the latent space. By effectively learning and transferring representations from HQ to LQ images, UDA-inversion shows promising results, outperforming some supervised methods. This study offers a unique inspiration for latent embedding distributions in image processing tasks.

## ACKNOWLEDGMENT

We would like to thank Haichao Shi and Yaru Zhang for their insightful discussions during the course of this project. This work was supported by the National Natural Science Foundation of China (NSFC) (Grant 62376265).

## REFERENCES

- [1] Ian J. Goodfellow, Jean Pouget-Abadie, Mehdi Mirza, et al., “Generative adversarial nets,” in *Advances in Neural Information Processing Systems (NIPS)*, 2014, pp. 2672–2680.
- [2] Tero Karras, Timo Aila, Samuli Laine, et al., “Progressive growing of gans for improved quality, stability, and variation,” in *International Conference on Learning Representations (ICLR)*, 2018.
- [3] Tero Karras, Samuli Laine, and Timo Aila, “A style-based generator architecture for generative adversarial networks,” in *IEEE Conference on Computer Vision and Pattern Recognition (CVPR)*, 2019, pp. 4401–4410.
- [4] Tero Karras, Samuli Laine, Miika Aittala, et al., “Analyzing and improving the image quality of stylegan,” in *IEEE Conference on Computer Vision and Pattern Recognition (CVPR)*, 2020, pp. 8107–8116.
- [5] Erik Härkönen, Aaron Hertzmann, Jaakko Lehtinen, et al., “Ganspace: Discovering interpretable GAN controls,” in *Advances in Neural Information Processing Systems (NIPS)*, 2020, vol. 33, pp. 9841–9850.
- [6] Yujun Shen, Jinjin Gu, Xiaoou Tang, et al., “Interpreting the latent space of gans for semantic face editing,” in *IEEE Conference on Computer Vision and Pattern Recognition (CVPR)*, 2020, pp. 9240–9249.
- [7] Zongze Wu, Dani Lischinski, and Eli Shechtman, “StyleSpace analysis: Disentangled controls for stylegan image generation,” in *IEEE Conference on Computer Vision and Pattern Recognition (CVPR)*, 2021, pp. 12863–12872.

- [8] Weihao Xia, Yulun Zhang, Yujiu Yang, et al., “Gan inversion: A survey,” *IEEE Transactions on Pattern Analysis and Machine Intelligence (TPAMI)*, pp. 1–17, 2022.
- [9] Kyoungkook Kang, Seongtae Kim, and Sunghyun Cho, “GAN inversion for out-of-range images with geometric transformations,” in *International Conference on Computer Vision (ICCV)*, 2021, pp. 13921–13929.
- [10] Jiapeng Zhu, Yujun Shen, Deli Zhao, et al., “In-domain GAN inversion for real image editing,” in *European Conference on Computer Vision (ECCV)*, 2020, pp. 592–608.
- [11] Elad Richardson, Yuval Alaluf, Or Patashnik, et al., “Encoding in style: A stylegan encoder for image-to-image translation,” in *IEEE Conference on Computer Vision and Pattern Recognition (CVPR)*, 2021, pp. 2287–2296.
- [12] Tianyi Wei, Dongdong Chen, Wenbo Zhou, et al., “E2style: Improve the efficiency and effectiveness of stylegan inversion,” *IEEE Transactions on Image Processing (TIP)*, pp. 3267–3280, 2022.
- [13] Yanbo Wang, Chuming Lin, Donghao Luo, et al., “High-resolution gan inversion for degraded images in large diverse datasets,” in *AAAI Conference on Artificial Intelligence (AAAI)*, 2022.
- [14] Rameen Abdal, Yipeng Qin, and Peter Wonka, “Image2stylegan: How to embed images into the stylegan latent space?,” in *International Conference on Computer Vision (ICCV)*, 2019, pp. 4431–4440.
- [15] Jinjin Gu, Yujun Shen, and Bolei Zhou, “Image processing using multi-code GAN prior,” in *IEEE Conference on Computer Vision and Pattern Recognition (CVPR)*, 2020, pp. 3009–3018.
- [16] Xingang Pan, Xiaohang Zhan, Bo Dai, et al., “Exploiting deep generative prior for versatile image restoration and manipulation,” *IEEE Transactions on Pattern Analysis and Machine Intelligence (TPAMI)*, pp. 262–277, 2021.
- [17] Xueqi Hu, Qiusheng Huang, Zhengyi Shi, et al., “Style transformer for image inversion and editing,” in *IEEE Conference on Computer Vision and Pattern Recognition (CVPR)*, 2022, pp. 11337–11346.
- [18] Tengfei Wang, Yong Zhang, Yanbo Fan, et al., “High-fidelity gan inversion for image attribute editing,” in *IEEE Conference on Computer Vision and Pattern Recognition (CVPR)*, 2022, pp. 11379–11388.
- [19] David Acuna, Guojun Zhang, Marc T Law, et al., “f-domain adversarial learning: Theory and algorithms,” in *International Conference on Machine Learning (ICML)*, 2021, pp. 66–75.
- [20] Chen Gong, Qiang He, Yunpeng Bai, et al., “The  $f$ -divergence reinforcement learning framework,” *arXiv preprint arXiv:2109.11867*, 2021.
- [21] Richard Zhang, Phillip Isola, Alexei A. Efros, et al., “The unreasonable effectiveness of deep features as a perceptual metric,” in *IEEE Conference on Computer Vision and Pattern Recognition (CVPR)*, 2018, pp. 586–595.
- [22] Jiankang Deng, Jia Guo, Niannan Xue, et al., “Arcface: Additive angular margin loss for deep face recognition,” in *IEEE Conference on Computer Vision and Pattern Recognition (CVPR)*, 2019, pp. 4690–4699.
- [23] Alexander B. Jung, Kentaro Wada, Jon Crall, et al., “imgaug,” <https://github.com/aleju/imgaug>, 2020, Online; accessed 01-Feb-2020.
- [24] Liyuan Liu, Haoming Jiang, Pengcheng He, et al., “On the variance of the adaptive learning rate and beyond,” *International Conference on Learning Representations (ICLR)*, 2020.
- [25] Michael Zhang, James Lucas, Jimmy Ba, et al., “Lookahead optimizer: k steps forward, 1 step back,” *Advances in Neural Information Processing Systems (NIPS)*, vol. 32, 2019.
- [26] Zhou Wang, Alan C. Bovik, Hamid R. Sheikh, et al., “Image quality assessment: from error visibility to structural similarity,” *IEEE Transactions on Image Processing (TIP)*, vol. 13, no. 4, pp. 600–612, 2004.
- [27] Martin Heusel, Hubert Ramsauer, Thomas Unterthiner, et al., “Gans trained by a two time-scale update rule converge to a local nash equilibrium,” in *Advances in Neural Information Processing Systems (NIPS)*, 2017, pp. 6626–6637.
- [28] Yuge Huang, Yuhang Wang, Ying Tai, et al., “Curricularface: Adaptive curriculum learning loss for deep face recognition,” in *IEEE Conference on Computer Vision and Pattern Recognition (CVPR)*, 2020, pp. 1–8.
- [29] Xiaoming Li, Chaofeng Chen, Shangchen Zhou, et al., “Blind face restoration via deep multi-scale component dictionaries,” in *European Conference on Computer Vision (ECCV)*, 2020.
- [30] Tao Yang, Peiran Ren, Xuansong Xie, et al., “Gan prior embedded network for blind face restoration in the wild,” in *IEEE Conference on Computer Vision and Pattern Recognition (CVPR)*, 2021, pp. 672–681.
- [31] Syed Mumtaz Ali and Samuel D Silvey, “A general class of coefficients of divergence of one distribution from another,” *Journal of the Royal*

*Statistical Society: Series B (Methodological)*, vol. 28, no. 1, pp. 131–142, 1966.

- [32] Xianjie Zhang, Yu Liu, Xiujuan Xu, et al., “Structural relational inference actor-critic for multi-agent reinforcement learning,” *Neuro-computing*, vol. 459, pp. 383–394, 2021.
- [33] XuanLong Nguyen, Martin J. Wainwright, and Michael I. Jordan, “Estimating divergence functionals and the likelihood ratio by convex risk minimization,” *IEEE Transactions on Information Theory*, vol. 56, no. 11, pp. 5847–5861, 2010.
- [34] Jonathan Krause, Michael Stark, Jia Deng, et al., “3d object representations for fine-grained categorization,” in *International Conference on Computer Vision Workshop (ICCVW)*, 2013, pp. 554–561.

# Appendix of GAN Inversion for Image Editing via Unsupervised Domain Adaptation

## APPENDIX A DETAILS OF PROOF

In this section, we provide the proofs for the mentioned theorem and equations in the main article.

### A. The lower bound of $f$ -divergence.

First, we recall the definition of  $f$ -divergence, from which we exploit a discrepancy to measure the difference between two distributions.

*Definition 1 ( $f$ -divergence [31]):* The  $f$ -divergence  $D_\phi$  measures the difference between two distributions  $P_s$  and  $P_t$  with densities  $p_s$  and  $p_t$ , where  $p_s$  is absolutely continuous with respect to  $p_t$ . The function  $\phi: \mathbb{R}_+ \rightarrow \mathbb{R}$  must be a convex, lower semi-continuous function and satisfy  $\phi(1) = 0$ . The  $f$ -divergence is formulated as:

$$D_\phi(P_s||P_t) = \int p_t(x)\phi\left(\frac{p_s(x)}{p_t(x)}\right) dx. \quad (9)$$

Many popular divergences used in machine learning are special cases of  $f$ -divergence. For instance, the KL-divergence  $D_{\text{KL}}(P||Q) := \mathbb{E}_{x \sim P}[\log(p(x)/q(x))]$  is the most commonly used one [1], [20], [32]. TABLE V lists popular divergences and convex functions. However,  $f$ -divergence can not be estimated for an arbitrary distribution from finite samples. Acuna et al. [19] propose a method to approximate  $f$ -divergence.

*Definition 2 ( $D_{h,\mathcal{H}}^\phi$  discrepancy [19]):* Under the same conditions of the convex function as Definition 1, let  $\phi^*$  be the Fenchel conjugate function of  $\phi$ , which is defined as  $\phi^*(y) := \sup_{x \in \mathbb{R}_+} \{xy - \phi(x)\}$ . The discrepancy between  $P_s$  and  $P_t$  can be formulated as:

$$D_{h,\mathcal{H}}^\phi(P_s||P_t) := \sup_{h' \in \mathcal{H}} |\mathbb{E}_{x \sim P_s} [\ell(h(x), h'(x))] - \mathbb{E}_{x \sim P_t} [\phi^*(\ell(h(x), h'(x)))]|. \quad (10)$$

In the above equation,  $\mathcal{H}$  is the hypothesis class. For any  $h$  and  $h' \in \mathcal{H}$ ,  $f$ -divergence and discrepancy  $D_{h,\mathcal{H}}^\phi$  satisfy the following inequality:

$$D_\phi(P_s||P_t) \geq D_{h,\mathcal{H}}^\phi(P_s||P_t). \quad (11)$$

*Proof.*

$$D_{h,\mathcal{H}}^\phi(P_s||P_t) = \sup_{h' \in \mathcal{H}} |\mathbb{E}_{x \sim P_s} [\ell(h(x), h'(x))] - \mathbb{E}_{x \sim P_t} [\phi^*(\ell(h(x), h'(x)))]| \quad (12)$$

$$\geq |\mathbb{E}_{x \sim P_s} [\ell(h(x), h'(x))] - \mathbb{E}_{x \sim P_t} [\phi^*(\ell(h(x), h'(x)))]| \quad (13)$$

$$\geq |\mathbb{E}_{x \sim P_s} [\ell(h(x), h'(x))] - \mathbb{E}_{x \sim P_t} [\phi^*(\ell(h(x), h'(x)))]| \quad (14)$$

$$= |\mathbb{E}_{x \sim P_s} [\ell(h(x), h'(x))] - \mathbb{E}_{x \sim P_t} [\phi^*(\ell(h(x), h'(x)))]| \quad (15)$$

$$= |\mathbb{E}_{x \sim P_s} [\ell(h(x), h'(x))] - \mathbb{E}_{x \sim P_t} [\phi^*(\ell(h(x), h'(x)))]| \quad (16)$$

$f$ -divergences have the low bound [33]:

$$D_\phi(P_s||P_t) \geq \sup_{T \in \mathcal{T}} \mathbb{E}_{x \sim P_s} [T(x)] - \mathbb{E}_{x \sim P_t} [\phi^*(T(x))]. \quad (17)$$

Equality in (17) holds if  $\mathcal{T}$  is measurable function set [19].  $\mathcal{T}$  was restricted by the definition of  $D_{h,\mathcal{H}}^\phi(P_s||P_t)$ , thus  $D_\phi(P_s||P_t) \geq D_{h,\mathcal{H}}^\phi(P_s||P_t)$ .  $\square$

### B. Theorem 1.

We suppose  $\ell: \mathcal{Y} \times \mathcal{Y} \rightarrow [0, 1] \subset \text{dom } \phi^*$ . Denote  $\lambda^* := R_s^\ell(h^*) + R_t^\ell(h^*)$ , and  $h^*$  is the ideal joint hypothesis. The error in the target domain is bounded by three terms:

$$R_t^\ell(h) \leq R_s^\ell(h) + D_{h,\mathcal{H}}^\phi(P_s||P_t) + \lambda^*. \quad (18)$$

*Proof.* From the definition of Fenchel conjugate, we have

$$\phi^*(t) = \sup_{x \in \text{dom } \phi} (xt - \phi(x)) \geq t - \phi(1) = t. \quad (19)$$

In this paper,  $R_t^\ell(h, f_t) = \ell(f_t(\mathbf{x}), G \circ E(\mathbf{x})) = \mathbb{E}_{\mathbf{x} \sim p_t} \|H(f_t(\mathbf{x})) - H(G \circ E(\mathbf{x}))\|_2$  satisfies triangle inequality. This allows us to derive

$$\begin{aligned} R_t^\ell(h, f_t) &\leq R_t^\ell(h, h^*) + R_t^\ell(h^*, f_t) && \text{triangle inequality} \\ &= R_t^\ell(h, h^*) + R_t^\ell(h^*, f_t) \\ &\quad - R_s^\ell(h, h^*) + R_s^\ell(h, h^*) \\ &\leq R_t^{\phi^* \circ \ell}(h, h^*) - R_s^\ell(h, h^*) \\ &\quad + R_s^\ell(h, h^*) + R_t^\ell(h^*, f_t) \\ &\leq |R_t^{\phi^* \circ \ell}(h, h^*) - R_s^\ell(h, h^*)| \\ &\quad + R_s^\ell(h, h^*) + R_t^\ell(h^*, f_t) \\ &\leq D_{h,\mathcal{H}}^\phi(P_s||P_t) + R_s^\ell(h, h^*) \\ &\quad + R_t^\ell(h^*, f_t) \\ &\leq D_{h,\mathcal{H}}^\phi(P_s||P_t) \\ &\quad + \underbrace{R_s^\ell(h, f_s) + R_s^\ell(h^*, f_s) + R_t^\ell(h^*, f_t)}_{\lambda^*}. \end{aligned} \quad (16)$$

Furthermore, if  $h^*$  is the ideal hypothesis, then  $\lambda^*$  is expected to be a rather small value.  $\square$

### C. Proposition 1.

Let us assume that  $\forall h \in \mathcal{H}, \exists h' \in \mathcal{H}$  s.t.  $\hat{\ell}(h'(\mathbf{w}), h(\mathbf{w})) = \phi'(\frac{p_s^w(\mathbf{w})}{p_t^w(\mathbf{w})})$ ,  $\forall z \in \text{supp}(p_t^w(\mathbf{w}))$ . The maximizing solution of  $d_{s,t}$  is  $D_{h,\mathcal{H}}^\phi(P_s^w||P_t^w)$ , i.e.,  $\max_{h' \in \mathcal{H}} d_{s,t} = D_{h,\mathcal{H}}^\phi(P_s^w||P_t^w)$ . *Proof.*

$$\begin{aligned} d_{s,t} &= \mathbb{E}_{\mathbf{w} \sim P_s^w} [\hat{\ell}(h'(\mathbf{w}), h(\mathbf{w}))] \\ &\quad - \mathbb{E}_{\mathbf{w} \sim P_t^w} [(\phi^* \circ \hat{\ell})(h'(\mathbf{w}), h(\mathbf{w}))] \\ &= \int p_t^w(\mathbf{w}) \left[ \frac{p_s^w(\mathbf{w})}{p_t^w(\mathbf{w})} \hat{\ell}(h'(\mathbf{w}), h(\mathbf{w})) - (\phi^* \circ \hat{\ell})(h'(\mathbf{w}), h(\mathbf{w})) \right] d\mathbf{w}. \end{aligned}$$

From the definition of Fenchel conjugate  $\phi^*$ , we have:

$$x \in \partial\phi^*(t) \iff \phi(x) + \phi^*(t) = xt \iff \phi'(x) = t. \quad (20)$$

Let  $t = \hat{\ell}(h(\mathbf{w}), h'(\mathbf{w}))$ , and  $x = \frac{p_s^w(\mathbf{w})}{p_t^w(\mathbf{w})}$ , then  $\forall \mathbf{w} \in \text{supp}(p_t^w(\mathbf{w}))$ , plugging  $\mathbf{w}$  into (20):

$$\begin{aligned} \hat{\ell}(h'(\mathbf{w}), h(\mathbf{w})) &= \phi'(p_s^w(\mathbf{w})/p_t^w(\mathbf{w})) \\ &\iff p_s^w(\mathbf{w})/p_t^w(\mathbf{w}) \in \partial\phi^*(\hat{\ell}(h'(\mathbf{w}), h(\mathbf{w}))). \end{aligned}$$

Suppose  $\hat{\ell}$  satisfies above condition, and the equality in (17) holds. Thus  $\max_{h' \in \mathcal{H}} d_{s,t} = D_\phi(P_s^w||P_t^w)$ .  $\square$

TABLE V: Common  $f$ -divergences and the corresponding convex function  $\phi$ .

Divergence	Convex Function $\phi(x)$	$\phi'(1)$
Kullback-Leibler	$x \log x$	1
Jensen-Shannon	$-(x+1) \log \frac{1+x}{2} + x \log x$	0
Pearson $\chi^2$	$(x-1)^2$	0
Total Variation	$\frac{1}{2} x-1 $	$[-0.5, 0.5]$

#### D. Choice Pearson $\chi^2$ divergence

Domain adaptation aims to minimize the discrepancy between two domains, which implies  $p_s^w(\mathbf{w})/p_t^w(\mathbf{w})$  closing to 1 and the discrepancy closing to 0, for all  $\mathbf{w} \in \text{supp}(p_t^w(\mathbf{w}))$ .

Maximizing  $d_{s,t}$  is equivalent to calculating  $D_\phi(P_s^w||P_t^w)$ , when  $D_\phi(P_s^w||P_t^w) \rightarrow 0$  implies  $\hat{\ell}(\hat{h}'(\mathbf{w}), \hat{h}(\mathbf{w})) \rightarrow 0$  and Proposition 1 supposes that the convex function  $\phi$  satisfies  $\phi'(1) = 0$ . Recall that common examples of  $f$ -divergence and the convex functions in TABLE V. We notice that the Pearson  $\chi^2$  divergence satisfies  $\phi'(1) = 0$ . Hence, Pearson  $\chi^2$  divergence is chosen to calculate  $d_{s,t}$  in this research.

Following Proposition 1, the formulation for calculating the discrepancy  $D_{h,\mathcal{H}}^\phi(P_s^w||P_t^w)$  is as follows:

$$D_{h,\mathcal{H}}^\phi(P_s^w||P_t^w) = \max_{h' \in \mathcal{H}} \mathbb{E}_{\mathbf{w} \sim P_s^w} [\hat{\ell}(h', h)] - \mathbb{E}_{\mathbf{w} \sim P_t^w} [(\phi^* \circ \hat{\ell})(h', h)]. \quad (21)$$

Intuitively, regarding  $G$  as the hypothesis function  $h$  and  $E$  maps images to latent space, the discrepancy is rewritten as:

$$\max_{G'} \mathbb{E}_{\mathbf{x} \sim P_s} [\hat{\ell}(G' \circ E, G \circ E)] - \mathbb{E}_{\mathbf{x} \sim P_t} [(\phi^* \circ \hat{\ell})(G' \circ E, G \circ E)]. \quad (22)$$

If we utilize an auxiliary generator  $G'$  to estimate the divergence and L2 loss as  $\hat{\ell}$  in (22), only optimizing the loss function in pixel level is insufficient to measure the difference between two images. In addition, the network structure of  $G'$  is the same as the generator  $G$  [4], leaving a larger amount of redundant model parameters.

To efficiently measure the similarity between two images and decrease parameters, we project inverted images into the representation space of LPIPS [21] to obtain the perceptual similarity between two images. Thus, the discrepancy is reformulated as:

$$\max_{\hat{H}} d_{s,t} = \mathbb{E}_{\mathbf{x} \sim P_s} [\hat{\ell}(\hat{H} \circ G \circ E, H \circ G \circ E)] - \mathbb{E}_{\mathbf{x} \sim P_t} [(\phi^* \circ \hat{\ell})(\hat{H} \circ G \circ E, H \circ G \circ E)], \quad (23)$$

where  $\hat{\ell}$  refers to LPIPS loss which is interpreted as to minimize the discrepancy at the perceptual feature-level, and  $\hat{H}$  indicates a network of the same structure as  $H$  in LPIPS loss. We summarize the proposed method in Algorithm 1.

---

#### Algorithm 1 Pseudo-code of UDA-inversion

---

**Input:**  $\mathbf{x}_s$ : image from source domain,  $\mathbf{x}_t$ : image from target domain,  $G(\cdot)$ : pre-trained generator,  $E(\cdot)$ : encoder,  $\hat{H}(\cdot)$ : feature extracting network,  $T$ : the total number of iterations.

**Initialization:** initialize  $E^{(0)}$ ,  $\hat{H}^{(0)}$ .

**For**  $t = 1, 2, 3, \dots, T$  **do**

1. Calculate  $d_{s,t}$ .
2. Update  $\hat{H}^{(t+1)}$  by ascending gradient:  $\partial d_{s,t} / \partial \hat{H}^{(t)}$ .
3. Compute  $\mathcal{L}_s$  and  $d_{s,t}$ .
4.  $\mathcal{L} = \mathcal{L}_s + \lambda_{uda} d_{s,t}$ .
5. Update  $E^{(t+1)}$  by descending gradient:  $\partial \mathcal{L} / \partial E^{(t)}$ .

**Output:**  $E^{(T)}$ : the well trained encoder for GAN inversion.

---

## APPENDIX B

### EXPERIMENTAL DETAILS AND RESULTS

#### A. Datasets and degradation operator

Here, we provide additional details about datasets and degradation operations to obtain images in target domains.

FFHQ dataset contains 70,000 high-quality images. We use the first 35,000 images [3] as the source domain, and the last 35,000 images are degraded as the target domain. In Stanford Cars dataset [34], we also use 50% images from the training set as the source domain, and the rest of images are degraded as the target domain. Analogous to existing GAN inversion methods [10], [12], [18], we resize the facial image resolution from  $1024^2$  to  $256^2$  and the car image resolution from  $512 \times 384$  to  $256 \times 192$  during training.

The target domain consists of perturbed images (i.e., LQ images)  $\mathbf{x}_t$ , which are degraded from HQ images  $\mathbf{x}_s$ :  $\mathbf{x}_t = \Psi(\mathbf{x}_s)$ , where  $\Psi$  denotes a degradation operation. The degradation operations contain rain layer, random mask, and down-sample, some of which are utilized in existing methods [11], [12]. Particularly, we utilized the ‘RainLayer’ feature from the imgaug library [23] with default parameters, perturbing images to a rain effect. We employ the same free-form mask generation algorithm as GPEN [30] and the same bicubic down-sample with the factor of 2 as E2style [12].

#### B. Evaluation Metrics

We quantitatively evaluate the inversion results from two aspects, i.e., inversion accuracy and image quality [8]. Inversion accuracy is usually measured by PSNR (Peak Signal-to-Noise Ratio), SSIM (Structural Similarity) [26], and MSE (Mean Squared Error). Images generated based on GANs are usually evaluated by FID (Fréchet inception distance) [27] to assess the quality and diversity of generated distribution.

#### C. Implementation and Hyper-parameters

We use the pre-trained StyleGAN2 [4] as the generator in experiments and adopt the encoder structure of HFGI [18], containing a basic encoder  $E_0$  and a consultation fusion branch to improve  $E_0$  with higher fidelity. The hyper-parameters of our encoder network are the same as HFGI. In addition, we follow existing encoder-based methods [12], [18] with Ranger

Face		Car	
Parameters	Value	Parameters	Value
$\lambda_1$	1	$\lambda_1$	1
$\lambda_2$	0.8	$\lambda_2$	0.8
$\lambda_3$	1	$\lambda_3$	1
$\lambda_4$	0.1	$\lambda_4$	0.1
$\lambda_{uda}$	1	$\lambda_{uda}$	0.5
Batch size	8	Batch size	12
Iteration	200,000	Iteration	100,000

TABLE VI: Hyper-parameters for our methods training on face and car dataset.

optimizer [24], [25] during training and set the initial learning rate to 0.0001. Two popular editing methods, GANSpace [5] and InterfaceGAN [6] are selected for semantic editing to manipulate inverted images.

All experiments are implemented on NVIDIA TITAN RTX GPUs. The hyper-parameters for the face dataset and car dataset are listed in TABLE VI.